Modeling and Tracking Phase and Frequency Offsets in Low-Precision Clocks

Radu David
ECE Department
Worcester Polytechnic Institute
Worcester, MA 01609
radud@wpi.edu

D. Richard Brown III
ECE Department
Worcester Polytechnic Institute
Worcester, MA 01609
drb@wpi.edu

Abstract—**This paper considers the problem of tracking carrier phase offsets in distributed multi-input multi-output (DMIMO) systems. Unlike conventional MIMO systems, each antenna in a DMIMO system is driven by an independent oscillator. To achieve coherent communication, e.g., distributed beamforming and/or nullforming, the time-varying offsets of these oscillators must be accurately tracked and compensated. While Kalman filtering has been used to optimally track phase and frequency offsets, it is well-known that the Kalman filter requires exact knowledge of the process and measurement noise parameters. This paper presents a general method for computing oscillator process and measurement noise parameters from an Allan variance characterization of the carrier phase offset measurements. Numerical results are presented using measured data from several N210 Universal Software Radio Peripherals (USRPs) at two different carrier frequencies. Using the estimated process and measurement noise parameters, the tracking performance is also evaluated on measured data from the USRPs and compared to theoretical predictions. Distributed beamforming and nullforming performance is also characterized using empirical phase prediction error statistics from the measured data.**

TABLE OF CONTENTS

1. INTRODUCTION

The last two decades have witnessed a fundamental shift in wireless communication systems away from single-antenna transceivers and toward Multi-Input Multi-Output (MIMO) communication. MIMO techniques have resulted in several important breakthroughs for wireless devices including increased range, increased spectral efficiency, reduced interference, and improved security. The theory and practice of MIMO communication has matured to the point where MIMO is now in several recent WiFi and cellular standards including 802.11n, 802.11ac, long-term evolution (LTE), WiMAX, and International Mobile Telecommunications (IMT)-Advanced. The applicability of MIMO techniques is often limited, however, by physical and economic constraints. For example, the form factor of handheld devices typically limits the number of antennas to only one or two. Consequently, the significant advantages of MIMO communication are simply not available to antenna- and/or cost-constrained devices.

While it is true that single-antenna devices are precluded from using MIMO communication techniques, it is also the case that these devices typically do not exist in isolation. Rather, single-antenna devices are often members of a network with many other single-antenna devices. If multiple devices in the network can coordinate their communication and pool their antenna resources, they can form a virtual antenna array and emulate a MIMO transceiver. This technique is called "distributed"-MIMO (DMIMO) or virtual-MIMO in the literature [1].

One well-studied example of DMIMO is distributed beamforming [2–6]. The goal in a distributed beamforming system is to control the phases and frequencies of the carriers at each transmit node so that the passband signals combine constructively at an intended receiver. Similarly, distributed nullforming systems use the degrees of freedom available from many transmit antennas to combine destructively in order to protect a receiver from interference [7–9]. Even in systems with time-invariant channels, the independent oscillators at each node in the distributed transmission system cause the effective channels between each transmitter and receiver to become time-varying.

It has been shown that tracking methods, e.g., Kalman filtering, can be quite effective at estimating and predicting the time-varying phase and frequency offsets in each independent transmit/receive oscillator pair and, consequently, in enabling distributed beamforming with devices using low-cost oscillators [10,11]. It is well-known, however, that the Kalman filter requires exact knowledge of the process and measurement noise parameters. In the context of tracking carrier phase offsets, the Kalman filter must have exact knowledge of the short-term and long-term stability parameters of the oscillators in the system as well exact knowledge of the statistics of the phase measurement error. While other methods for identifying the Kalman filter parameters for general systems have been proposed in literature [12], the method proposed here is specific to oscillator characterization.

In this paper, we present a general method for computing oscillator process and measurement noise parameters from an Allan variance characterization of the carrier phase offset measurements. We provide specific results for oscillators used in the N210 Universal Software Radio Peripheral (USRP) manufactured by Ettus research, as these devices are often used in experimental studies of DMIMO systems [13]. We also provide numerical results showing precise tracking of clock phase and frequency offsets between two USRP devices with a Kalman filter. In a system with periodic channel phase measurements, our results with a 15 MHz

This work was supported by the National Science Foundation awards CCF-1302104 and CCF-1319458.
978-1-4799-5380-6/15/$31.00

carrier frequency show that the RMS phase prediction error is less than 25 degrees at a observation period of 2 seconds. At a 900 MHz carrier frequency, the RMS phase prediction error is less than 25 degrees at a observation period of 50 ms. In both cases, the actual tracking performance is close to the performance predicted by the Kalman filter error covariance matrices. In addition, we provide beamforming and nullforming performance results using the empirical phase prediction error statistics from the measured data using the method described in [14]. We demonstrate a scenario with beamforming power towards an intended receiver within 1 dB of ideal while nulls of -5 dB to -30 dB are also steered towards protected receivers.

The remaining of this paper is organized as follows. In Section 2 we introduce the system model for oscillator dynamics and describe the Allan variance used for parameter estimation. In Section 3, our experimental setup and data analysis methodology are explained. Section 4 provides the results of our experiments and analysis. We conclude the paper with Section 5.

2. System Model

Oscillator Dynamics

The transmit and receive nodes in the system are assumed to have independent local oscillators. These local oscillators have inherent frequency offsets and behave stochastically, causing phase offset variations in the effective channel from the transmit node to the receive node even when the propagation channels are otherwise time invariant. This section describes a discrete-time dynamic model to characterize the dynamics of the carrier phase and frequency variations between a transmitter and receiver in the DMIMO system.

Based on the two-state models in [15, 16], we define the discrete-time state of the transmit node's carrier as $\boldsymbol{x}_t[k] = [\phi_t[k], \omega_t[k]]^\top$ where $\phi_t[k]$ and $\omega_t[k]$ correspond to the carrier phase and frequency offsets in radians and radians per second, respectively, at the transmit node with respect to an ideal carrier phase reference. The state update of the transmit node's carrier is then

$$\boldsymbol{x}_t[k+1] = \boldsymbol{F}(T)\boldsymbol{x}_t[k] + \boldsymbol{u}_t[k] \tag{1}$$

with

$$\boldsymbol{F}(T) = \begin{bmatrix} 1 & T \\ 0 & 1 \end{bmatrix} \tag{2}$$

where T is an arbitrary sampling period selected to be small enough to avoid phase aliasing at the largest expected frequency offsets.

The process noise vector $\boldsymbol{u}_t[k] \overset{\text{i.i.d.}}{\sim} \mathcal{N}(\boldsymbol{0}, \boldsymbol{Q}(T))$ causes the carrier derived from the local oscillator at the transmit node to deviate from an ideal linear phase trajectory. The covariance of the discrete-time process noise is derived from a continuous-time model in [15]:

$$\boldsymbol{Q}(T) = \omega_c^2 T \begin{bmatrix} q_1 + q_2\frac{T^2}{3} & q_2\frac{T}{2} \\ q_2\frac{T}{2} & q_2 \end{bmatrix} \tag{3}$$

where ω_c is the nominal common carrier frequency in radians per second and q_1 (units of seconds) and q_2 (units of Hertz) are the process noise parameters corresponding to white frequency noise and random walk frequency noise, respectively.

The receive node in the system also has an independent local oscillator used to generate the carrier for down-mixing and is governed by the same dynamics as (1) with state $\boldsymbol{x}_r[k]$, process noise $\boldsymbol{u}_r[k] \overset{\text{i.i.d.}}{\sim} \mathcal{N}(\boldsymbol{0}, \boldsymbol{Q}(T))$, and process noise parameters q_1 and q_2 as in (3).

Since the receive node can only measure the relative phase and frequency of the transmit node after propagation, we define the *pairwise offset* after propagation as

$$\boldsymbol{\delta}[k] = \begin{bmatrix} \phi[k] \\ \omega[k] \end{bmatrix} = \boldsymbol{x}_t[k] + \begin{bmatrix} \psi \\ 0 \end{bmatrix} - \boldsymbol{x}_r[k].$$

Note that $\boldsymbol{\delta}[k]$ is governed by the state update

$$\boldsymbol{\delta}[k+1] = \boldsymbol{f}(T)\boldsymbol{\delta}[k] + \boldsymbol{u}_t[k] - \boldsymbol{u}_r[k]. \tag{4}$$

where $\boldsymbol{f}(T)$ is given in (2).

We assume observations are received with an observation period $T_0 = MT$ where M is a positive integer. We further assume that the observations are so short as to only provide useful phase estimates. The observations can be expressed as

$$y[k] = \boldsymbol{H}[k]\delta[k] + v[k] \tag{5}$$

where

$$\boldsymbol{H}[k] = \begin{cases} [1, 0] & k = 0, M, 2M, \ldots \\ [0, 0] & \text{otherwise} \end{cases} \tag{6}$$

and $v[k] \overset{\text{i.i.d.}}{\sim} \mathcal{N}(0, r)$ is the measurement noise which is assumed to be independent of the process noise. The problem then is to accurately estimate the parameters $\{q_1, q_2, r\}$ to facilitate tracking of the pairwise phase and frequency offsets in each channel. The following section introduces the concept of Allan variance, a method for characterizing oscillator stability that can be used to estimate the relevant parameters.

Allan Variance

The Allan variance characterizes the short-term and long-term behavior of the frequency offset of an oscillator [17]. The Allan variance is defined using the expectation formula:

$$\sigma_y^2(\tau) = \frac{1}{2} < (\dot{\phi}_{avg}(t+\tau) - \dot{\phi}_{avg}(t))^2 > \tag{7}$$

where

$$\dot{\phi}_{avg} = \frac{1}{\tau}\int_{t-\tau}^{t} \dot{\phi}(t')\,dt' = \frac{1}{\tau}[\phi(t) - \phi(t-\tau)] \tag{8}$$

with $\dot{\phi}(t)$ as the instantaneous frequency offset and $\phi(t)$ as the phase offset. This represents a measure of the frequency stability of an oscillator over a given averaging interval τ. In [18], it is shown that the Allan variance as a function of the averaging time τ follows $\sigma_y^2(\tau) = \frac{q_1}{\tau} + \frac{q_2\tau}{3}$, where q_1 and q_2 are the respective short term and long term frequency stability parameters used in (3).

In addition to these two parameters, the measurement noise variance r is also required for the two-state model. This can also be estimated from the Allan variance, as it has an effect on the short term measurements. Fig. 1 shows an example of the impact of measurement noise on the Allan deviation plot. The measurement noise acts as white phase noise rather than white frequency noise and its effect scales proportionally to τ^{-2} in the Allan variance measurement [19].

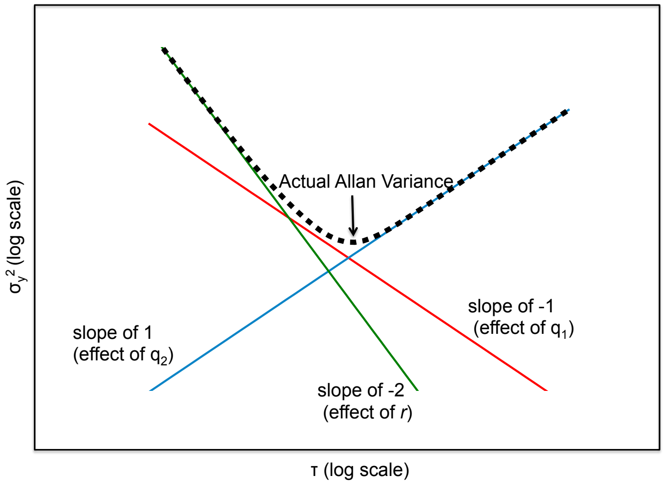

Figure 1. The effect of white phase noise on Allan variance.

Hence, to jointly estimate the process and measurement noise parameters (q_1, q_2, r), we can perform a least-squares fit the empirically-estimated Allan variance to the equation

$$\sigma_y^2(\tau) = \frac{3r}{\tau^2} + \frac{q_1}{\tau} + \frac{q_2\tau}{3}. \tag{9}$$

As can be seen in Fig. 1, the measurement noise can have a significant impact on the Allan variance measurements, to the point where the short term stability parameter q_1 is completely obscured by the measurement noise. Nevertheless, a least squares fit can still provide an upper bound on the q_1 parameter.

3. Methodology

The results in this paper are based on experimental data gathered with the USRP N210 software defined radio platform. These devices are designed for RF communications and are commonly used in research and academic settings as well as for rapid development in industrial and defense applications [20]. The platform contains an FPGA used to stream data between the device and a host computer and it has the ability to operate from DC to 6 GHz via interchangeable daughterboards. The intended use is for the host computer to handle the baseband processing and to configure the RF parameters, while the upconversion/downconversion and the filters required to bring the signals to RF frequencies are performed by the device.

Data Acquisition

The USRPs used in the experiments had the FPGA configured to upconvert/downconvert I/Q data and to interface with the host computer. The interchangeable daughterboards that are used to reach different carrier frequency bands have a frequency range of $1\ \mathrm{MHz} - 250\ \mathrm{MHz}$. Fig. 2 shows the main components of the experimental setup. All the experiments in this paper were performed with the USRPs connected by a coaxial cable to eliminate any effects such as multipath and time-varying channel dynamics and to focus only on the carrier phase and frequency dynamics of the USRPs.

Rather than using a separate sampler to record the signals generated by the USRP hardware, our system uses two USRPs with separate but otherwise identical oscillators. By using identical oscillators, the combined effect of the two independent but otherwise identical oscillators is statistically twice the effect of just one oscillator, i.e., the effective process noise covariance is twice that of a single oscillator. This allows us to statistically characterize the process noise parameters of an individual USRP oscillator.

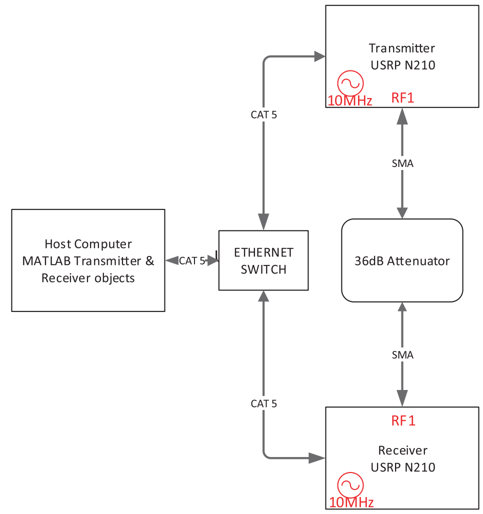

Figure 2. Experimental setup for data acquisition.

The ethernet port allows for gigabit ethernet data transfer between the USRP and the host computer. This connection allows for real time data gathering and analysis even at high sampling rates. The USRP internal clock is a single 10MHz oscillator that is converted to the desired carrier frequencies using PLLs.

The transmit power of the USRP was measured to be approximately $-2\ \mathrm{dBm}$ and an attenuator of $36\ \mathrm{dB}$ was placed on the wired communication link to achieve $-38\ \mathrm{dBm}$ of receive power. The main steps of the experiment are shown below, together with the description of the waveforms at each of the steps.

1. Generate a complex tone at a baseband frequency f so that the baseband signal is

$$s_t[k] = A_t e^{j2\pi f k} \tag{10}$$

where A_t is the transmitter gain.
2. The transmit USRP modulates the tone with the specified carrier frequency and transmits it over the wire. The transmitted signal is given as

$$w[k] = A_t \cos((2\pi(f + f_c)k + \phi_t[k])) \tag{11}$$

where $\phi_t[k]$ represents the time-varying phase offset introduced by the transmitter.
3. The receive USRP demodulates the received tone, samples it and sends it to the host computer. The resulting baseband signal is given as

$$\begin{aligned} s_r[k] &= A_t g A_r e^{j(2\pi((f+f_c)-f_c)k+\phi_t[k]-\phi_r[k]+\psi)} \\ &= A e^{j(2\pi f k+\phi[k])} \end{aligned} \tag{12}$$

where g is the channel gain, A_r is the receiver gain, and $\phi[k] = \phi_t[k] - \phi_r[k] + \psi$ represents the total transmitter-receiver phase offset, including the channel propagation phase ψ. In practice, this measurement will be corrupted by noise which is modeled as the observation in (5). Thus, our observation will be $y[k] = \phi[k] + v[k]$.

4. The received complex data is stored on the host computer in double precision floating point format for further analysis.

We performed experiments at two nominal carrier frequencies: 15 MHz and 900 MHz. In both cases, the baseband tone frequency was set to $f = 2000$ Hz and the baseband sampling frequency at the receiver was set to $f_s = 100 \times 10^6/512$ MHz $= 195,312.5$ Hz. In the 15 MHz experiments, the *Basic TX* and *Basic RX* USRP daughter boards were used and in the 900 MHz experiments, the *SBX* USRP daughter boards were used [21].

The baseband sampling frequency at the receiver was selected to avoid aliasing. Based on earlier experiments, the largest recorded frequency offset on the USRP N210s we observed was approximately 45 kHz at a 900 MHz carrier frequency, and less than 1 kHz for a carrier frequency of 15 MHz. The USRP hardware uses a 12-bit ADC with a nominal sampling frequency of 100 MHz that can be later decimated by any value between 4 and 512 leading to the minimum sampling frequency of $100\text{ MHz}/512 = 195,312.5$ Hz. This sampling frequency was used for all of our experiments.

All data processing is done on the host computer connected to the N210 USRPs via gigabit ethernet cables. Transmitter and receiver objects are instantiated in MATLAB on two separate USRPs. The transmit radio is configured to transmit the 2000Hz complex tone and the receive radio is configured to demodulate the data and save it as a complex variable. The duration of each experiment was approximately ten minutes.

Data Analysis

By taking the unwrapped phase from the complex baseband signal in (12) and removing the linear frequency trend, we obtain the zero mean phase offset progression. This is the $\phi[k]$ term that we use in our Allan variance characterization of the oscillators, and subsequent evaluation of the tracking performance.

Kalman Filter Tracking

Based on the 2-state model described in Section 2, we can implement a Kalman filter to track and predict the phase offset given periodic observations. Note that the Kalman filter specified below is updated at the sampling period T while observations are received with period $T_0 = MT$. The one-step state prediction $\hat{\delta}[k+1|k]$ is given as

$$\hat{\boldsymbol{\delta}}[k+1|k] = \boldsymbol{F}(T)\hat{\boldsymbol{\delta}}[k|k] \tag{13}$$

with state estimate

$$\hat{\boldsymbol{\delta}}[k|k] = \hat{\boldsymbol{\delta}}[k|k-1] + \boldsymbol{K}[k](y[k] - \boldsymbol{H}[k]\hat{\boldsymbol{\delta}}[k|k-M]). \tag{14}$$

The Kalman gain is given as

$$\boldsymbol{K}[k] = \boldsymbol{\Sigma}[k|k-1]\boldsymbol{H}^\top[k](\boldsymbol{H}[k]\boldsymbol{\Sigma}[k|k-1]\boldsymbol{H}^\top[k] + r)^{-1}.$$

The quantity $\boldsymbol{\Sigma}[k|k-1]$ denotes the one-step prediction error covariance matrix (ECM) which is used in the computation of the estimation error covariance matrix as

$$\boldsymbol{\Sigma}[\boldsymbol{k}|\boldsymbol{k}] = \boldsymbol{\Sigma}[k|k-1] - \boldsymbol{K}[k]\boldsymbol{H}[k]\boldsymbol{\Sigma}[k|k-1] \tag{15}$$

with the Kalman filter recursion

$$\boldsymbol{\Sigma}[k+1|k] = \boldsymbol{F}(T)\boldsymbol{\Sigma}[k|k]\boldsymbol{F}(T)^\top + \boldsymbol{Q}(T) \tag{16}$$

Note that the process noise covariance $\boldsymbol{Q}(T)$ accounts for the effect of the process noise at both the transmitter and at the receiver. Given measurements at sample instants $k = 0, M, 2M, \ldots,$ we denote the Kalman filter's MMSE phase prediction at sample instant $\ell > k$ as $\hat{\phi}[\ell\,|\,k]$.

Finally, to evaluate the performance of our tracking mechanism, we compare the error between the actual phase measurements $y[\ell]$ and the predictions $\hat{\phi}[\ell\,|\,k]$ with the ECM result $\boldsymbol{\Sigma}[k+\ell|k]$. The squared phase measurement errors are averaged over multiple runs of the Kalman filter to obtain an empirical estimate of the steady-state behavior.

4. Numerical Results

This section presents the numerical results outlining the process of obtaining accurate Kalman Filter parameters and the performance evaluation of our implementation. All the analysis is performed on real data obtained from the USRP N210 platform and prediction errors are computed with respect to the measurements. The empirically-estimated prediction variances are also compared to the variances provided by the Kalman filter's error covariance matrices.

Fig. 3 shows examples of unwrapped phase offset realizations for multiple experiments. This data was detrended and decimated by a factor of 125. As expected, these results show the significant phase variations caused by the stochastic behavior of the independent oscillators in the system.

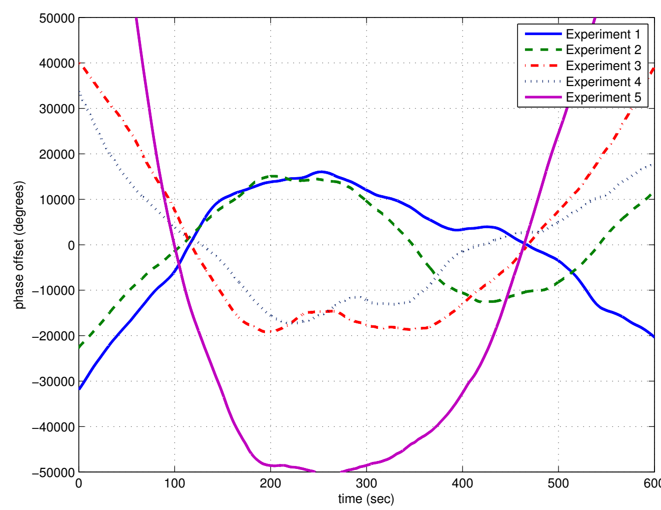

Figure 3. Experimental unwrapped phase offsets between two USRP N210 nodes at 15 MHz.

The phase offset data is then used in the calculation of Allan deviation and subsequent parameter estimation. Fig. **??** illustrates the individual effect of measurement noise and short and long term stability parameters on the Allan deviation result. It can be seen that the measurement noise has a large impact on the short term measurements, making the q_1 parameter difficult to estimate.

Table 1 shows the range of parameters that were determined over five separate experiments. The q_1 and q_2 parameters in the table are divided by 2 in order to account for the effect of both the transmitter and receiver clocks. This is due to the combining of the noise process of the two nodes, as shown in (4).

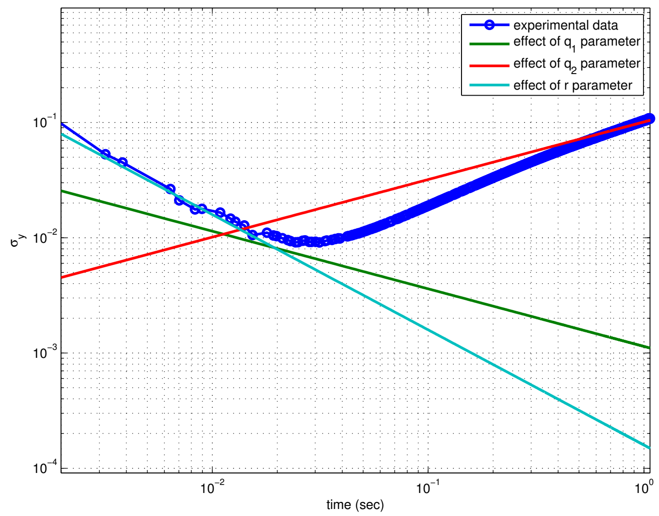

Figure 4. Least-squares parameter fit with experimental Allan deviation results.

Parameter	units	min value	max value
r	rad^2	1.6×10^{-8}	3.3×10^{-8}
q_1	sec	1.4×10^{-22}	3.02×10^{-21}
q_2	Hz	2.62×10^{-18}	6.31×10^{-18}

Table 1. Parameter ranges estimated over five separate experiments.

15 MHz Phase Tracking and Prediction Experiments

Figure 5 shows the RMS phase prediction error of a Kalman filter tracker compared to the RMS prediction error from the Kalman filter's error covariance matrix. This result shows that at a observation period of $T_0 = 2$ seconds, the maximum RMS phase prediction error is less than 25 degrees after the Kalman filter achieves steady-state. In addition, the plot shows that the phase prediction error is consistent with the performance predictions from the Kalman filter error covariance matrix.

By varying the observation period T_0, it is possible to get an idea of the expected phase offset error and to choose the value that meets the phase offset requirements of a given system. The Kalman filter phase prediction performance is plotted with respect to the observation period T_0 in Fig. **??**. These results show that the RMS phase prediction error with measured data is quite close to the error covariance matrix predictions.

To better understand the meaning of these results in the context of distributed transmission systems, we show the performance of a hypothetical distributed transmission system with $N_t = 10$ transmitters and $N_r = 1$ receiver. In [14], theoretical beamforming and nullforming power gains are derived and shown to only depend on the phase variance.

Fig. 7 shows the expected beamforming power of the system given the phase error of the empirically estimated phase offset predictions. The figure shows a loss of less than 1 dB in beamforming power when $T_0 = 2$ seconds. In Fig. 8, it is shown that the nullforming power has a steeper drop as expected from the theoretical steady-state results. In practice, observation periods on the order of of milliseconds

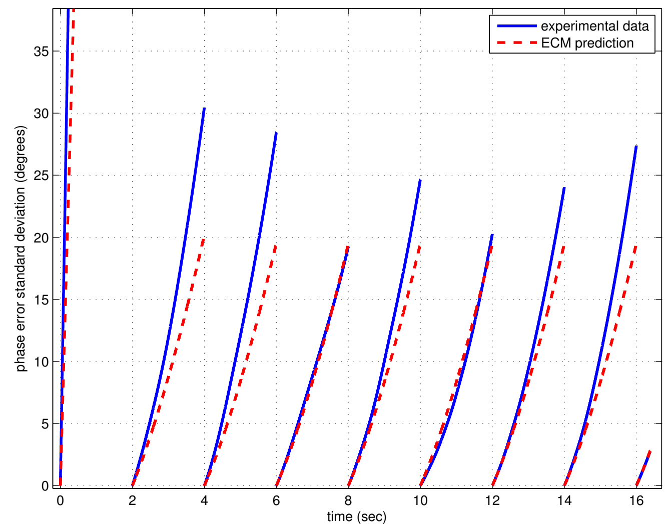

Figure 5. Kalman filter RMS phase error at 15 MHz with observation period $T_0 = 2$ seconds.

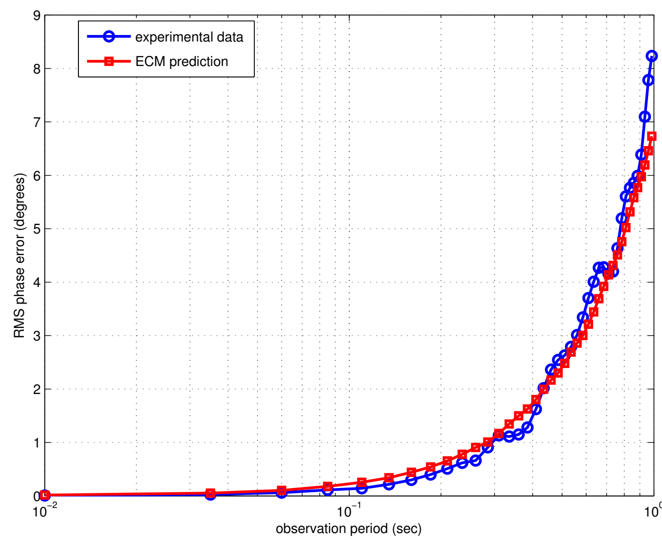

Figure 6. RMS phase error: experimental data and ECM predictions versus observation period T_0 at 15 MHz.

are feasible, leading to very good performance at a carrier frequency of 15 MHz, but also leading to increased feedback overhead.

900 MHz Phase Tracking and Prediction Experiments

In this section, we provide experimental tracking results for phase tracking between two USRP N210s at a 900 MHz carrier frequency. The increase in carrier frequency from 15 MHz to 900 MHz leads to a much larger process noise covariance matrix and, consequently, requires a smaller observation period T_0 to provide satisfactory performance. The Kalman filter phase tracking and prediction performance assuming an observation period of $T_0 = 50$ ms is shown in Fig. 9 below. The corresponding beamforming and nullforming expected power is shown in Figs. 10 and 11.

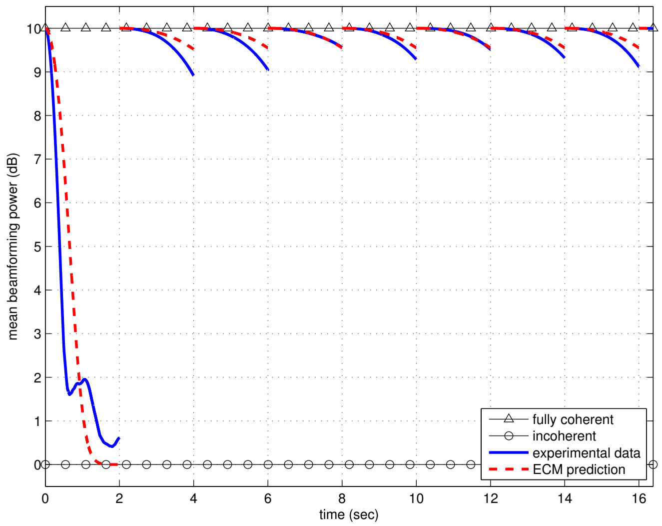

Figure 7. Expected beamforming power at 15 MHz with observation period $T_0 = 2$ seconds..

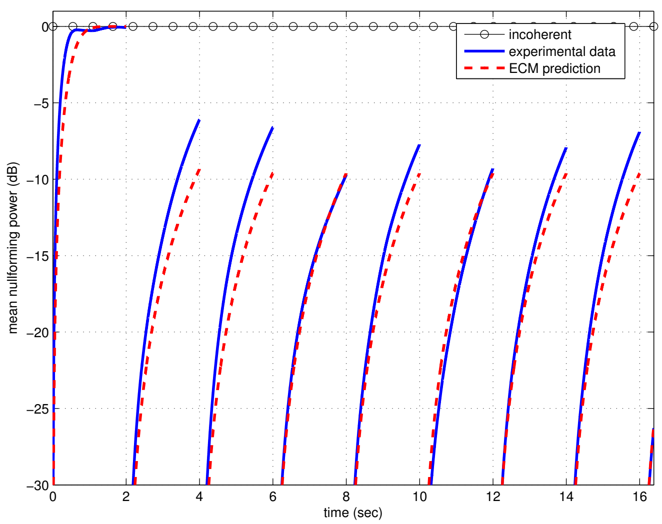

Figure 8. Expected nullforming power at 15 MHz with observation period $T_0 = 2$ seconds..

5. Conclusions

In this paper we showed a method for extracting measurement and process noise parameters to facilitate oscillator tracking in a Kalman filtering framework. We tested our method on experimental data obtained from phase offset measurements between two USRP N210 devices. By closely matching the Kalman Filter parameters to the experimental data, we show that we can achieve very good tracking performance. Our results show that parameter estimation is not straightforward since the Allan deviation results are influenced by measurement noise. Nevertheless, the results show that the phase error of the Kalman filter output translates into very good beamforming and nullforming performance, even for practical observation periods. Moreover, the experimental results agree closely with the Kalman filter error covariance matrices.

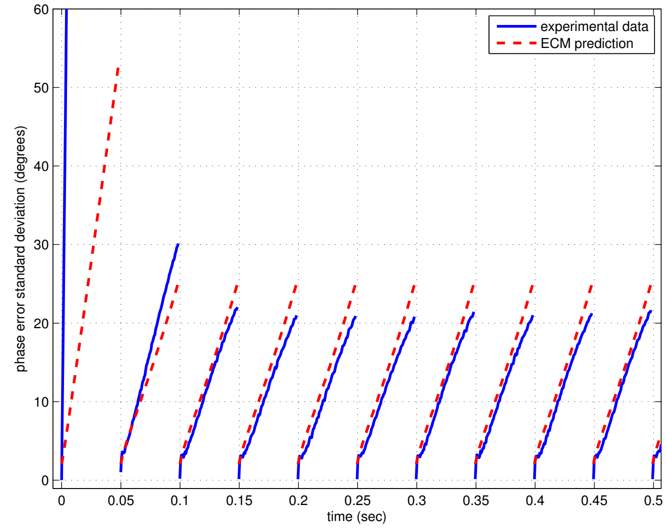

Figure 9. Kalman filter RMS phase error at 900 MHz with observation period $T_0 = 50$ ms.

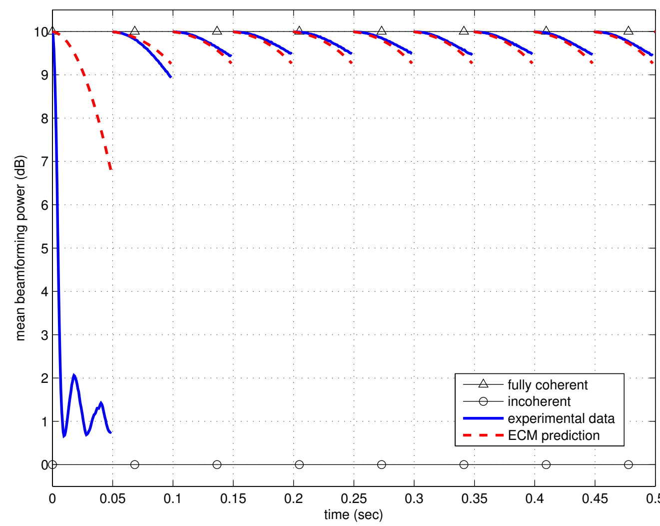

Figure 10. Expected beamforming power at 900MHz with observation period $T_0 = 50$ ms.

References

[1] M. Dohler, A. Gkelias, and H. Aghvami, "A resource allocation strategy for distributed mimo multi-hop communication systems," *Communications Letters, IEEE*, vol. 8, no. 2, pp. 99–101, Feb 2004.

[2] R. Mudumbai, G. Barriac, and U. Madhow, "On the feasibility of distributed beamforming in wireless networks," *IEEE Trans. on Wireless Communications*, vol. 6, no. 5, pp. 1754–1763, May 2007.

[3] R. Mudumbai, D.R. Brown III, U. Madhow, and H.V. Poor, "Distributed transmit beamforming: Challenges and recent progress," *IEEE Comm. Mag.*, vol. 47, no. 2, pp. 102–110, Feb. 2009.

[4] R. Preuss and D. Brown, "Retrodirective distributed transmit beamforming with two-way source synchronization," in *Information Sciences and Systems (CISS), 2010 44th Annual Conference on*, march 2010, pp. 1 –6.

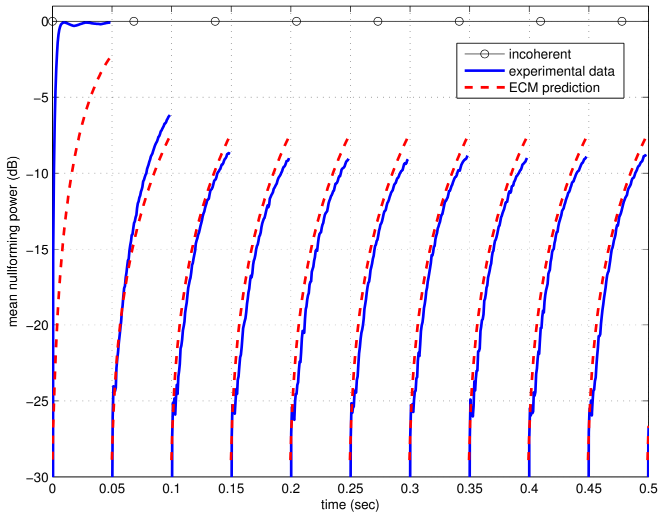

Figure 11. Expected nullforming power at 900MHz with observation period $T_0 = 50$ ms.

[5] R. Preuss and D.R. Brown III, "Two-way synchronization for coordinated multi-cell retrodirective downlink beamforming," *IEEE Trans. Signal Proc.*, vol. 59, no. 11, pp. 5415–27, Nov. 2011.

[6] D. Brown, P. Bidigare, and U. Madhow, "Receiver-coordinated distributed transmit beamforming with kinematic tracking," in *Acoustics, Speech and Signal Processing (ICASSP), 2012 IEEE International Conference on*, Mar. 2012, pp. 5209–5212.

[7] K. Zarifi, S. Affes, and A. Ghrayeb, "Collaborative null-steering beamforming for uniformly distributed wireless sensor networks," *IEEE Trans. on Signal Processing*, vol. 58, no. 3, pp. 1889 –1903, Mar. 2010.

[8] D.R. Brown III and U. Madhow, "Receiver-coordinated distributed transmit nullforming with channel state uncertainty," in *Conf. Inf. Sciences and Systems (CISS2012)*, Mar. 2012, to appear.

[9] D.R. Brown III, P. Bidigare, S. Dasgupta, and U. Madhow, "Receiver-coordinated zero-forcing distributed transmit nullforming," in *Statistical Signal Processing Workshop (SSP), 2012 IEEE*, Aug. 2012, pp. 269–272.

[10] H. Kim, X. Ma, and B. R. Hamilton, "Tracking low-precision clocks with time-varying drifts using kalman filtering," *IEEE/ACM Trans. Netw.*, pp. 257–270, 2012.

[11] G. Giorgi and C. Narduzzi, "Performance analysis of kalman-filter-based clock synchronization in ieee 1588 networks," *IEEE T. Instrumentation and Measurement*, pp. 2902–2909, 2011.

[12] R. Mehra, "On the identification of variances and adaptive kalman filtering," *Automatic Control, IEEE Transactions on*, vol. 15, no. 2, pp. 175–184, Apr 1970.

[13] F. Quitin, U. Madhow, M. Rahman, and R. Mudumbai, "Demonstrating distributed transmit beamforming with software-defined radios," in *World of Wireless, Mobile and Multimedia Networks (WoWMoM), 2012 IEEE International Symposium on a*, June 2012, pp. 1–3.

[14] D. Brown and R. David, "Receiver-coordinated distributed transmit nullforming with local and unified tracking," in *Acoustics, Speech and Signal Processing (ICASSP), 2014 IEEE International Conference on*, May 2014, pp. 1160–1164.

[15] L. Galleani, "A tutorial on the 2-state model of the atomic clock noise," *Metrologia*, vol. 45, no. 6, pp. S175–S182, Dec. 2008.

[16] G. Giorgi and C. Narduzzi, "Performance analysis of kalman filter-based clock synchronization in IEEE 1588 networks," in *International IEEE Symposium on Precision Clock Synchronization for Measurement, Control, and Communication*, October 12-16 2009, pp. 1–6.

[17] D. Allan, "Time and frequency (time-domain) characterization, estimation, and prediction of precision clocks and oscillators," *Ultrasonics, Ferroelectrics, and Frequency Control, IEEE Transactions on*, vol. 34, no. 6, pp. 647–654, Nov 1987.

[18] C. Zucca and P. Tavella, "The clock model and its relationship with the allan and related variances," *Ultrasonics, Ferroelectrics and Frequency Control, IEEE Transactions on*, vol. 52, no. 2, pp. 289 –296, feb. 2005.

[19] "Characterization of frequency and phase noise," Report 580 of the International Radio Consultative Committee (C.C.I.R), Tech. Rep., 1986.

[20] (2015, Jan.) Usrp n210. [Online]. Available: https://www.ettus.com/product/details/UN210-KIT

[21] (2014, Jun.) Rf daughterboards. [Online]. Available: https://www.ettus.com/product/details/BasicTX

BIOGRAPHY

Radu David *received his B.S. in Electrical and Computer Engineering from Worcester Polytechnic Institute in 2010 and M.S. degree in Electrical and Computer Engineering from Carnegie Mellon University in 2012. He is currently a Ph.D. student at Worcester Polytechnic Institute. His research interests are in distributed communication systems, oscillator stability, and Multiple-input Multiple-output systems.*

D. Richard Brown III *received the B.S. and M.S. degrees in Electrical Engineering from The University of Connecticut in 1992 and 1996, respectively, and received the Ph.D. degree in Electrical Engineering from Cornell University in 2000. From 1992-1997, he was with General Electric Electrical Distribution and Control. He joined the faculty at Worcester Polytechnic Institute (WPI) in Worcester, Massachusetts in 2000 and currently is an Associate Professor. He also held an appointment as a Visiting Associate Professor at Princeton University from August 2007 to June 2008. His research interests are currently in coordinated wireless transmission and reception, synchronization, distributed computing, and game-theoretic analysis of communication networks.*